Structure scaling properties of confined nematic polymers in plane Couette cells: The weak flow limit

M. Gregory Forest[a)]

Department of Mathematics, University of North Carolina at Chapel Hill, Chapel Hill, North Carolina 27599-3250

Qi Wang

Department of Mathematics, Florida State University, Tallahassee, Florida 32306

Hong Zhou

Department of Applied Mathematics and Statistics, University of California at Santa Cruz, Santa Cruz, California 95064

Ruhai Zhou

Department of Mathematics, University of North Carolina at Chapel Hill, Chapel Hill, North Carolina 27599-3250

(Received 8 July 2003; final revision received 17 September 2003)

Synopsis

One of the confounding issues in laminar flow processing of nematic polymers is the generation of molecular orientational structures on length scales that remain poorly characterized with respect to molecular and processing control parameters. For plane Couette flow within the Leslie–Ericksen continuum model, theoretical results since the 1970s yield two fundamental predictions about the length scales of nematic distortion: a power law scaling behavior, Er^{-p}, $\frac{1}{4} \leqslant p \leqslant 1$, where Er is the Ericksen number (ratio of viscous to elastic stresses); the exponent p varies according to whether the structure is a localized boundary layer or an extended structure. Until now, comparable results which incorporate molecular elasticity (i.e., distortions in the shape of the orientational distribution) have not been derived from mesoscopic Doi–Marrucci–Greco (DMG) tensor models. In this paper, we derive asymptotic, one-dimensional gap structures, along the flow-gradient direction, in ''slow'' Couette cells, which reflect self-consistent coupling between the primary flow, in-plane director (nematic) and order parameter (molecular) elasticity, and confinement conditions (plate speeds, gap height, and director anchoring angle). We then read off the small Deborah number, viscoelastic structure predictions: The flow is simple shear. The orientation structures consist of: two molecular-elasticity boundary layers with the Marrucci scaling $\mathrm{Er}^{-1/2}$, which are amplified by tilted plate anchoring; and a nonuniform, director-dominated structure that spans the entire gap, with Er^{-1} average length scale, present for any anchoring angle. We close with direct numerical simulations of the DMG steady, flow-nematic boundary-value problem, first to benchmark the small Deborah number structure formulas, and then to document onset of new flow-orientation structures as the asymptotic expansions become disordered. © *2004 The Society of Rheology.* [DOI: 10.1122/1.1626676]

[a)]Electronic mail: forest@math.unc.edu

I. INTRODUCTION

Laminar flow processing of nematic polymer films and molds is plagued by the generation of molecular orientational structures on length scales that remain poorly understood. These structures impart nonuniform material properties, which are believed to compromise performance features. Absent of a characterization of nematic mesostructures with respect to molecular and processing control parameters, e.g., in the form of structure scaling properties, a systematic study of the mesostructure–material property relationships cannot even begin.

The experimental documentation of micron-scale textures [cf. Larson and Mead (1992, 1993); Donald and Windle (1992); Burghardt (1998); Larson (1999); the recent review by Tan and Berry (2003)] has compelled many theoretical and numerical efforts [cf. the recent review by Rey and Denn (2002)] to explain and simulate the dominant structure scales. The dimensional analysis of de Gennes (1974), Marrucci (1991), and Marrucci and Greco (1993) in plane Couette flow, using the continuum Leslie–Ericksen (LE) theory, produces a similarity length scale $L_M \sim \mathrm{Er}^{-1/2}$, where Er is the Ericksen number, which measures viscous effects relative to distortional elasticity. The linearized analysis of Carlsson (1986) on the LE model characterizes a boundary penetration length consistent with the Marrucci scaling. Larson (1993), Larson and Mead (1992, 1993) focused on roll-cell structures, experimentally and theoretically, which obey power law behavior between $\mathrm{Er}^{-1/4}$ and $\mathrm{Er}^{-1/2}$. Important early results included exact solutions derived by Manneville (1981), Carlsson (1984), and the provocative concept of director turbulence [cf. Cladis and Torza (1976)].

For nematic polymers, it is necessary to go beyond the LE model and allow for molecular elasticity as well as nematic director structures. (In terms of the second-moment orientation tensor, this translates to eigenvalue as well as eigenvector variations.) Absent of flow or other applied fields, the authors [Forest *et al.* (2000, 2001)] derived families of exact steady-state and traveling-wave solutions of a Doi–Marrucci–Greco mesoscopic tensor model. These free-space solutions yield a variety of layered and domain-wall structures, and translate to familiar light-intensity patterns. They are intrinsic nematic polymer structures that reflect a balance between the short-range molecular elasticity potential (of Maier–Saupe form) and the intermediate-range distortional elasticity potential [of Marrucci and Greco (1991)]. Furthermore, these intrinsic states arise either from optical axis distortions with frozen order parameter values (consistent with a LE structure), or from order-parameter-dominated orientational distortions. Lacking an applied field such as shear flow and absent of confinement conditions such as plate anchoring, these families of structures have no selection mechanisms, either in which types of solutions are resonated or in length scales of the structures. It is reasonable to surmise that local plate anchoring conditions, and local flow type and rate, provide selection criteria for order-parameter versus director-dominated structure modes, and furthermore, provide local and long-range length-scale selection criteria through stress and torque balances.

In confined plane Couette cell flows, numerical studies on various mesoscopic Doi–Marrucci–Greco (DMG) mesoscopic tensor models [Tsuji and Rey (1997); Sgalari *et al.* (2002); Kupferman *et al.* (2000)] remain inconclusive with respect to the Marrucci scaling or related power law behavior. This is not surprising: the parameter space is too large; each mesoscopic model corresponds to a different mesoscopic closure approximation of the Doi kinetic theory [cf. Forest and Wang (2003)]; each model uses a variation on the Marrucci–Greco distortional elasticity potential; the choices of spatial dimensionality of both flow and orientation relative to the flow axes vary; and finally, the coupling of flow

versus imposed flow during structure evolution are both explored. Given the added complexity of accurate numerical solvers in confined geometries, comparisons are difficult, and conclusions regarding structure scaling properties remain elusive.

Given this appraisal, we are motivated toward three goals: to extend de Gennes' and Marrucci's dimensional analysis at the equation level to asymptotic construction of families of exact solutions, with flow and confinement providing selection of length scales and of the structure type (cf. boundary layers versus structures that span the entire shear gap); to extend Carlsson's linearized analysis of plate confinement conditions to fully nonlinear orientational structure properties and scaling behavior, especially to identify whether structure length scales inherit dependence on the gap width; and to identify scaling behavior of the order parameters as well as directors, each free to interact according to the flow-nematic-confinement balance equations.

We consider a DMG mesoscopic tensor model, allowing a full coupling between flow structure and director (nematic) & order parameter (molecular) distortions, and with imposed plate motion and molecular anchoring conditions. The model, based on the Doi closure, has been benchmarked in the longwave, monodomain regime and small Deborah number limit with simulations of the Doi kinetic theory at nematic concentrations [Forest *et al.* (2003)], and the pure nematic equations support the families of inherent structures noted earlier [Forest *et al.* (2000, 2001)]. The effect of closure rule, which strongly affects monodomain response to shear flow [cf. Forest and Wang (2003)], will be highlighted when we reach the results of our analysis. In short, the structures we predict are robust to closure, but prefactors vary with the mesoscopic Leslie tumbling parameter, which varies with closure.

Following Marrucci and Carlsson, we describe one-dimensional spatial structures that form in the gap between parallel plates moving oppositely at prescribed constant speeds, with mesoscopic molecular anchoring conditions at the plates. Likewise, *we assume an in-plane orientation tensor and posit that the velocity field varies only along the primary flow direction*. This assumption is not easily lifted; the out-of-plane analysis has thus far proven unwieldy. The structures and scaling properties we derive here are, therefore, not applicable to out-of-plane orientation behavior; the spatial analog of out-of-plane director tipping is a topic of current interest.

From this formulation, we develop a nonlinear asymptotic analysis in the slow-plate (small Deborah number) limit, which yields *exactly solvable, steady flow-nematic structures*. From the exact constructions, we simply read off length-scale selection criteria and structure scaling properties, explicitly in terms of molecular parameters (nematic concentration N, molecule aspect ratio r, persistence length l of distortional elasticity) and processing conditions [gap width $(2h)$, plate speeds $\pm v_0$, and plate anchoring conditions on the molecular field].

II. MODEL FORMULATION

We consider planar shear flow between two plates located at $y = \pm h$, in Cartesian coordinates (x,y,z), moving with corresponding velocity $\mathbf{v} = (\pm v_0,0,0)$, respectively. Figure 1 depicts the cross section of the shear flow on the (x,y) plane. Variations in the direction of flow (x) and primary vorticity direction (z), and transport in the vertical (y) direction are suppressed. There are *two apparent length scales*: the gap half-width h and the persistence length l of the distortional elasticity potential of Marrucci and Greco. The molecular parameter l is the mesoscopic analog of a Frank elasticity constant; we restrict

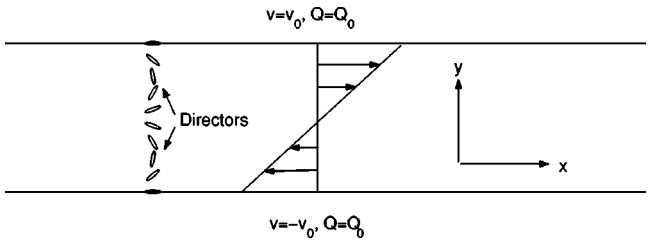

FIG. 1. Plane shear flow geometry. Nonslip boundary conditions for the velocity and boundary anchoring for the orientation tensor given by the stable nematic rest state are prescribed, with major director angle $\psi_0 = 0$ shown here. A schematic major director windup is shown across the shearing cell.

here to the one-constant approximation where bend, splay, and twist distortion constants are presumed equal. There are two obvious time scales in the model: a bulk flow time scale,

$$t_{\text{flow}} = \frac{h}{v_0}, \tag{1}$$

and a nematic time scale of average rotational diffusivity,

$$t_{\text{nematic}} = \frac{1}{6D_r}. \tag{2}$$

One can also form scales associated with solvent viscosity and the three nematic viscosities, but in the weak flow limit they correspond to higher order effects.

We nondimensionalize the coordinates, variables, model equations, and boundary conditions using the device scale h, the nematic time-scale t_{nematic}, and a characteristic stress $\tau_0 = \rho h^2/t_{\text{nematic}}^2$, where ρ is the liquid density:

$$\tilde{\mathbf{x}} = \frac{1}{h}\mathbf{x}, \quad \tilde{t} = \frac{t}{t_{\text{nematic}}}, \quad \tilde{\mathbf{v}} = \frac{t_{\text{nematic}}}{h}\mathbf{v}, \quad \tilde{\tau} = \frac{\tau}{\tau_0}, \quad \tilde{p} = \frac{p}{\tau_0}. \tag{3}$$

The following six dimensionless parameters arise in the flow-nematic equations:

$$\text{Re} = \frac{\tau_0 t_{\text{nematic}}}{\eta}, \quad \alpha = \frac{3ckT}{\tau_0}, \quad \text{Er} = \frac{8}{N}\frac{h^2}{l^2}, \quad \mu_i = \frac{3ckT\zeta_i}{t_{\text{nematic}}\tau_0}, \quad i = 1,2,3. \tag{4}$$

Re is the solvent Reynolds number; Er is the Ericksen number of the DMG model consistent with Kupferman *et al.* (2000), Feng *et al.* (2000); $\mu_i, i = 1,2$, and 3 are three nematic Reynolds numbers, and α is a normalized entropic parameter (c is a number density of nematic molecules, k is the Boltzmann constant, and T is absolute temperature).

Our scaling inserts the Deborah number De in the flow boundary condition, where we can efficiently impose the slow plate limit. Since $v_x(y = \pm h) = \pm v_0 = h/t_{\text{nematic}}\tilde{v}_x(\tilde{y} = \pm 1)$, the dimensionless axial velocity at the boundary is the ratio of the bulk flow rate v_0/h and nematic relaxation rate $6Dr$:

$$|\tilde{v}_x(\pm 1)| = \text{De} = \frac{v_0/h}{6Dr} = \frac{v_0\, t_{\text{nematic}}}{h}. \tag{5}$$

The latter equality provides another view on the slow plate limit, $0 < \text{De} \ll 1$. The plate velocity condition and nematic time scale define a flow direction scale, Δx

$= v_0 t_{\text{nematic}}$, the distance the plates move in the unit timescale of nematic relaxation. Then, De can be also written as

$$\text{De} = \frac{\Delta x}{h}, \tag{6}$$

which is the reciprocal slope of the standard linear shear velocity streamline picture. The asymptotic condition $0 < \text{De} \ll 1$ asserts the nematic relaxation time scale is much shorter than the bulk flow timescale, so that the plates move a short distance relative to the gap half-width over the timescale of molecular relaxation.

We hereafter drop the tilde $\sim$ on all quantities, using only *dimensionless scales and variables in all equations, solutions, and figures*. We note the *molecular aspect ratio r* of spheroidal molecules enters the Doi model through the dimensionless parameter

$$a = \frac{r^2-1}{r^2+1}.$$

The balance of linear momentum, stress constitutive equation, continuity equation, and the equation for the orientation tensor are

$$\frac{d\mathbf{v}}{dt} = \nabla\cdot(-p\mathbf{I}+\tau),$$

$$\begin{aligned}\tau = {} & \left(\frac{2}{\text{Re}}+\mu_3\right)\mathbf{D}+a\alpha F(\mathbf{Q})+\frac{a\alpha}{3\text{Er}}\left\{\Delta\mathbf{Q}:\mathbf{Q}\left(\mathbf{Q}+\frac{\mathbf{I}}{3}\right)-\frac{1}{2}(\Delta\mathbf{Q}\mathbf{Q}+\mathbf{Q}\Delta\mathbf{Q})-\frac{1}{3}\Delta\mathbf{Q}\right\}\\ & +\frac{\alpha}{3\text{Er}}\left\{\frac{1}{2}(\mathbf{Q}\Delta\mathbf{Q}-\Delta\mathbf{Q}\mathbf{Q})-\frac{1}{4}(\nabla\mathbf{Q}:\nabla\mathbf{Q}-\nabla\nabla\mathbf{Q}:\mathbf{Q})\right\}\\ & +\mu_1\left\{\left(\mathbf{Q}+\frac{\mathbf{I}}{3}\right)\mathbf{D}+\mathbf{D}\left(\mathbf{Q}+\frac{\mathbf{I}}{3}\right)\right\}+\mu_2\mathbf{D}:\mathbf{Q}\left(\mathbf{Q}+\frac{\mathbf{I}}{3}\right),\end{aligned}$$

$$\nabla\cdot\mathbf{v} = 0,$$

$$\begin{aligned}\frac{d}{dt}\mathbf{Q} = {} & \Omega\mathbf{Q}-\mathbf{Q}\Omega+a[\mathbf{D}\mathbf{Q}+\mathbf{Q}\mathbf{D}]+\frac{2a}{3}\mathbf{D}-2a\mathbf{D}:\mathbf{Q}\left(\mathbf{Q}+\frac{\mathbf{I}}{3}\right)\\ & -\frac{1}{\Lambda}\left\{F(\mathbf{Q})+\frac{1}{3\text{Er}}\left[\Delta\mathbf{Q}:\mathbf{Q}\left(\mathbf{Q}+\frac{\mathbf{I}}{3}\right)-\frac{1}{2}(\Delta\mathbf{Q}\mathbf{Q}+\mathbf{Q}\Delta\mathbf{Q})-\frac{1}{3}\Delta\mathbf{Q}\right]\right\},\end{aligned} \tag{7}$$

where

$$F(\mathbf{Q}) = (1-N/3)\mathbf{Q}-N\mathbf{Q}^2+N\mathbf{Q}:\mathbf{Q}(\mathbf{Q}+\mathbf{I}/3), \tag{8}$$

$$\Lambda = \begin{cases}1, & \text{with constant rotary diffusivity}\\ \left(1-\dfrac{3}{2}\mathbf{Q}:\mathbf{Q}\right)^2, & \text{with orientation-dependent rotary diffusivity.}\end{cases} \tag{9}$$

The boundary conditions for the scaled axial velocity v_x are

$$v_x(y = \pm 1) = \pm\text{De}. \tag{10}$$

We assume *homogeneous mesophase anchoring at the plates*, given by the quiescent stable nematic equilibrium,

$$\mathbf{Q}|_{y=\pm 1} = s_0\left(\mathbf{nn}-\frac{\mathbf{I}}{3}\right),$$

$$s_0 = \frac{1}{4}\left(1+3\sqrt{1-\frac{8}{3N}}\right), \tag{11}$$

where s_0 is the stable uniaxial order parameter specified by the nematic concentration $N > \frac{8}{3}$, and $\mathbf{n}$ is the equilibrium uniaxial director, assumed to lie in the shear plane (flow–flow gradient plane) at some experimentally dictated *anchoring angle* ψ_0 with respect to the flow direction,

$$\mathbf{n} = (\cos\psi_0, \sin\psi_0, 0). \tag{12}$$

The anchoring angle will appear prominently in the results below; plate preparations yield tangential ($\psi_0 = 0$), homeotropic ($\psi_0 = \pi/2$), or tilted ($0 < \psi_0 < \pi/2$) anchoring.

We consider the in-plane mesophase orientation of LCPs with two directors of $\mathbf{Q}$ confined to the shearing plane (x,y), but still admitting biaxiality. This constraint implies that two components in the matrix representation of $\mathbf{Q}$ must vanish, $Q_{xz} = Q_{yz} = 0$. Alternatively, the orientation tensor can be written in terms of directors and order parameters:

$$\mathbf{Q} = s(y,t)\left(\mathbf{nn}-\frac{\mathbf{I}}{3}\right)+\beta(y,t)\left(\mathbf{n}^{\perp}\mathbf{n}^{\perp}-\frac{\mathbf{I}}{3}\right), \tag{13}$$

with the directors $\mathbf{n},\mathbf{n}^{\perp}$ confined to the (x,y) plane and parametrized by the in-plane Leslie angle $\psi(y,t)$,

$$\mathbf{n} = (\cos\psi, \sin\psi, 0), \quad \mathbf{n}^{\perp} = (-\sin\psi, \cos\psi, 0). \tag{14}$$

The third director is rigidly constrained along the vorticity axis.

The explicit coordinate change between these $\mathbf{Q}$ representations is

$$Q_{xx} = s(\cos^2\psi-\tfrac{1}{3})+\beta(\sin^2\psi-\tfrac{1}{3}),$$

$$Q_{xy} = (s-\beta)\sin\psi\cos\psi,$$

$$Q_{yy} = s(\sin^2\psi-\tfrac{1}{3})+\beta(\cos^2\psi-\tfrac{1}{3}). \tag{15}$$

The Jacobian of the mapping $(s,\beta,\psi) \rightarrow (Q_{xx},Q_{xy},Q_{yy})$ is $\partial(Q_{xx},Q_{xy},Q_{yy})/\partial(s,\beta,\psi) = (\beta-s)/3$. Unless $s-\beta = 0$, which is a uniaxial limit, the mapping is nonsingular. We shall switch between these representations to extract properties of the orientation tensor.

With the biaxial representation (13) of $\mathbf{Q}$, the tensor equation in Eq. (7) can be written in terms of the order parameters (s,β) and the Leslie angle ψ:

$$\frac{\partial s}{\partial t} = -\frac{1}{\Lambda}\left\{U(s)+\frac{2N}{3}s\beta(1+\beta-s)+\frac{2}{9\mathrm{Er}}(s-\beta)g(s,\beta)\left(\frac{\partial\psi}{\partial y}\right)^2 + \frac{1}{9\mathrm{Er}}\left[-(1-s)(1-\beta+2s)\frac{\partial^2 s}{\partial y^2}+s(1-s+2\beta)\frac{\partial^2\beta}{\partial y^2}\right]\right\}+\frac{a}{3}\frac{\partial v_x}{\partial y}g(s,\beta)\sin 2\psi,$$

$$\frac{\partial \beta}{\partial t} = -\frac{1}{\Lambda}\left\{U(\beta)+\frac{2N}{3}s\beta(1+s-\beta)+\frac{2}{9\mathrm{Er}}(\beta-s)g(\beta,s)\left(\frac{\partial\psi}{\partial y}\right)^2 + \frac{1}{9\mathrm{Er}}\left[\beta(1-\beta+2s)\frac{\partial^2 s}{\partial y^2}-(1-\beta)(1-s+2\beta)\frac{\partial^2\beta}{\partial y^2}\right]\right\}-\frac{a}{3}\frac{\partial v_x}{\partial y}g(\beta,s)\sin 2\psi,$$

$$\frac{\partial\psi}{\partial t} = \frac{1}{6(s-\beta)}\left\{\frac{\partial v_x}{\partial y}[3\beta-3s+a(2+s+\beta)\cos 2\psi] + \frac{1}{3\mathrm{Er}\Lambda}(2+s+\beta)\left[(s-\beta)\frac{\partial^2\psi}{\partial y^2}+2\frac{\partial\psi}{\partial y}\left(\frac{\partial s}{\partial y}-\frac{\partial\beta}{\partial y}\right)\right]\right\}, \tag{16}$$

where

$$U(s) = s\left[1-\frac{N}{3}(1-s)(2s+1)\right], \tag{17}$$

$$g(s,\beta) = 1+3s\beta-\beta+2s-3s^2. \tag{18}$$

The momentum equation reduces to a single equation for the velocity component v_x,

$$\frac{\partial v_x}{\partial t} = \frac{\partial \tau_{xy}}{\partial y},$$

$$\tau_{xy} = \frac{a\alpha}{2}\left[U(s)-U(\beta)+\frac{4Ns\beta}{3}(\beta-s)\right]\sin 2\psi+\frac{a\alpha}{18\mathrm{Er}}\left[-h(s,\beta)\frac{\partial^2 s}{\partial y^2}+h(\beta,s)\frac{\partial^2\beta}{\partial y^2} + 2(s-\beta)[g(s,\beta)+g(\beta,s)]\left(\frac{\partial\psi}{\partial y}\right)^2\right]\sin 2\psi+\frac{a\alpha}{18\mathrm{Er}}(s+\beta+2)\left[(\beta-s)\frac{\partial^2\psi}{\partial y^2} - 2\left(\frac{\partial s}{\partial y}-\frac{\partial\beta}{\partial y}\right)\frac{\partial\psi}{\partial y}\right]\cos 2\psi+\frac{\alpha}{6\mathrm{Er}}(s-\beta)\left[(s-\beta)\frac{\partial^2\psi}{\partial y^2}+2\left(\frac{\partial s}{\partial y}-\frac{\partial\beta}{\partial y}\right)\frac{\partial\psi}{\partial y}\right] + \left[\frac{\mu_1}{6}(s+\beta+2)+\frac{\mu_2}{8}(s-\beta)^2(1-\cos 4\psi)+\frac{1}{\mathrm{Re}}+\frac{\mu_3}{2}\right]\frac{\partial v_x}{\partial y}, \tag{19}$$

where

$$h(s,\beta) = (1-\beta+2s)(1+\beta-s). \tag{20}$$

We seek steady solutions of the dimensionless governing Eqs. (16)–(20) subject to the boundary conditions

$$v_x|_{y=\pm 1} = \pm\mathrm{De}, \quad s|_{y=\pm 1} = s_0, \quad \beta|_{y=\pm 1} = 0, \quad \psi|_{y=\pm 1} = \psi_0. \tag{21}$$

We posit a formal asymptotic expansion in the small De number limit, consistent with the above boundary conditions:

$$v_x = \sum_{k=1}^{\infty} v_x^{(k)}(y)\mathrm{De}^k, \quad \psi = \sum_{k=0}^{\infty} \psi^{(k)}(y)\mathrm{De}^k,$$

$$s = \sum_{k=0}^{\infty} s^{(k)}(y)\mathrm{De}^k, \quad \beta = \sum_{k=1}^{\infty} \beta^{(k)}(y)\mathrm{De}^k. \tag{22}$$

Alternatively, the Cartesian representation of $\mathbf{Q}$ is expanded in the form:

$$\mathbf{Q} = \sum_{k=0}^{\infty} \mathbf{Q}^{(k)}(y)\mathrm{De}^k, \tag{23}$$

with $\mathbf{Q}^{(0)}$ a quiescent, homogeneous equilibrium given by Eq. (11). $\psi^{(1)}$, $s^{(1)}$, $\beta^{(1)}$ and the components of $\mathbf{Q}^{(1)}$ are explicitly related by

$$\psi^{(1)} = \frac{2Q_{xy}^{(1)}\cos 2\psi_0 - (Q_{xx}^{(1)} - Q_{yy}^{(1)})\sin 2\psi_0}{2s},$$

$$s^{(1)} = \tfrac{3}{2}(Q_{xx}^{(1)} + Q_{yy}^{(1)}) + \tfrac{1}{2}(Q_{xx}^{(1)} - Q_{yy}^{(1)})\cos 2\psi_0 + Q_{xy}^{(1)}\sin 2\psi_0,$$

$$\beta^{(1)} = \tfrac{3}{2}(Q_{xx}^{(1)} + Q_{yy}^{(1)}) - \tfrac{1}{2}(Q_{xx}^{(1)} - Q_{yy}^{(1)})\cos 2\psi_0 - Q_{xy}^{(1)}\sin 2\psi_0. \tag{24}$$

Notice that the anchoring conditions at the two moving plates are assumed identical, which presumes the shear cell begins from a quiescent, homogeneous, nematic equilibrium. This is consistent with tangential and normal anchoring conditions, and with tilted anchoring conditions if the plates are prepared so that the anchoring angles are equal rather than opposite sign. Different conditions at each plate require a non-homogeneous steady structure at leading order, which we will not pursue for this study.

A. Exact steady asymptotic structures

From either representation of $\mathbf{Q}$, the above expansions are inserted into the full system of flow-nematic equations, Eqs. (7)–(9) or (16)–(18), equations for the $O(\mathrm{De})$ and $O(\mathrm{De}^2)$ variables derived, and then systematically solved. We now state the results, following the notation in expansions (22) and (23).

- The *axial velocity* at $O(\mathrm{De})$, $v_x^{(1)}$, *reproduces the simple shear structure:*

$$v_x^{(1)} = y. \tag{25}$$

  This result gives some justification to the historical practice of imposing pure shear flow kinetics even in spatially non-uniform flows [Tsuji and Rey (1997); Rey and Denn (2002)] in order to decouple the momentum equation. For asymptotically ordered, in-plane structures in the low De limit, all nonlinearity in the flow profile is a perturbation of pure shear. We will return in the numerical section to onset of nonlinear flow profiles as the asymptotic solutions become invalid.
- The orientation tensor at $O(\mathrm{De})$, $\mathbf{Q}^{(1)}$, *decomposes into one extended structure that spans the entire gap and two boundary layer structures that are localized at the plates*:

$$\mathbf{Q}^{(1)} = \mathrm{Er}(y^2-1)\mathbf{Q}_1+\left(\frac{\cosh(\mathrm{Er}^{1/2}By)}{\cosh(\mathrm{Er}^{1/2}B)}-1\right)\mathbf{Q}_2+\left(\frac{\cosh(\mathrm{Er}^{1/2}Dy)}{\cosh(\mathrm{Er}^{1/2}D)}-1\right)\mathbf{Q}_3, \quad (26)$$

where

$$\mathbf{Q}_1 = -\frac{3a}{2\lambda_L}(1-\lambda_L\cos 2\psi_0)\begin{pmatrix}\sin 2\psi_0 & \cos 2\psi_0 & 0\\ \cos 2\psi_0 & -\sin 2\psi_0 & 0\\ 0 & 0 & 0\end{pmatrix}, \quad (27)$$

$$\mathbf{Q}_2 = \frac{a(1-s_0)^2(1+2s_0)}{36s_0}\sin 2\psi_0\begin{pmatrix}1-\cos 2\psi_0 & -\sin 2\psi_0 & 0\\ -\sin 2\psi_0 & 1+\cos 2\psi_0 & 0\\ 0 & 0 & -2\end{pmatrix}, \quad (28)$$

$$\mathbf{Q}_3 = -\frac{a(4s_0-1)}{4N(3N-8)s_0}\sin 2\psi_0\begin{pmatrix}1+3\cos 2\psi_0 & 3\sin 2\psi_0 & 0\\ 3\sin 2\psi_0 & 1-3\cos 2\psi_0 & 0\\ 0 & 0 & -2\end{pmatrix}, \quad (29)$$

with a the molecular geometry parameter, and the constants B,D,λ_L are given by

$$\lambda_L = \frac{a(2+s_0)}{3s_0}, \quad (30)$$

$$B = 3\sqrt{\frac{Ns_0}{1-s_0}}, \quad (31)$$

$$D = B\sqrt{\frac{4s_0-1}{3(1+2s_0)}}. \quad (32)$$

The parameters B and D are $O(1)$ constants, uniquely prescribed by the nematic concentration N; recall $s_0 = s_0(N)$ from Eq. (11), where $\frac{1}{4} < s_0 < 1$ for $\frac{8}{3} < N < \infty$.

The (y^2-1) term proportional to the tensor $\mathbf{Q}_1$ corresponds to an extended, nonuniform structure that spans the entire shear gap, which we call a *permeation structure* by contrast with the *boundary layer structures* proportional to $\mathbf{Q}_2$ and $\mathbf{Q}_3$, which are highly localized at the plates. In the sections below we decompose $\mathbf{Q}_1$, $\mathbf{Q}_2$, and $\mathbf{Q}_3$ into directors and order parameters in order to extract nematic and molecular elasticity scaling properties.

The parameter λ_L is the *mesoscopic Leslie tumbling parameter* corresponding to the Doi closure of kinetic theory [Kuzuu and Doi (1983, 1984); Marrucci (1991); Marrucci and Greco (1993); Forest and Wang (2003); Forest *et al.* (2003)]. The Leslie parameter traditionally arises as the critical bulk *dynamical diagnostic* [Doi and Edwards (1986); Beris and Edwards (1994); Larson (1999)]. If one were to close the Doi kinetic theory on second moments by use of other closure rules, e.g., Hinch and Leal (1972), Tsuji and Rey (1997), de Gennes and Prost (1993), Maffettone *et al.* (2000), the parameter λ_L *encodes the primary effect of closure rule on stationary spatial in-plane structures at low* De.

For any closure, *the prefactor* $(1-\lambda_L\cos 2\psi_0)$ *implies a remarkable temporal-to-spatial transference mechanism* associated with the permeation structure. Flow-alignment in time (i.e., $|\lambda_L| > 1$) leads to a tendency toward suppression of, whereas tumbling

bulk dynamics (i.e., $|\lambda| < 1$) promotes, this bulk spatial mode (since $(1-\lambda_L \cos 2\psi_0)$ is bounded away from zero). This result is the mesoscopic theory analog of Marrucci's analysis of the LE steady structures, where the Leslie tumbling parameter also arises [Marrucci (1991)].

The critical role of ψ_0, the plate anchoring angle, is apparent in *both boundary-layer tensors* $\mathbf{Q}_2$ *and* $\mathbf{Q}_3$, which *vanish for tangential* ($\psi_0 = 0$) *or normal* ($\psi_0 = \pi/2$) *anchoring*. Thus, these exact constructions imply *an arbitrary pre-tilt of* ψ_0 *away from the flow or flow-gradient directions will amplify boundary layers of strength equal to the nonlocal extended structure proportional to* $\mathbf{Q}_1$. This nonlocal structure, on the other hand, can be suppressed only if the nematic polymer is "flow-aligning," i.e., $\lambda_L > 1$, Eq. (30), and then by preparing the plate anchoring condition precisely parallel to the Leslie alignment angle, $\psi_0 = \frac{1}{2}\cos^{-1}(1/\lambda_L)$.

B. Director structure

In continuum LE theory, all elasticity is projected into the major director. The first consequence of these exact mesoscopic solutions is quite striking: *the director is seen to only participate in the long-range extended structure and to not vary in the boundary layers*. From Eq. (24), the director angle ψ is explicitly given by

$$\psi = \psi_0 + \mathrm{De}\,\psi^{(1)} + O(\mathrm{De}^2),$$

$$\psi^{(1)} = \mathrm{Er}\,M(y^2-1),$$

$$M[a,s_0(N),\psi_0] = \frac{9}{2(2+s_0)}[1-\lambda_L \cos(2\psi_0)]. \tag{33}$$

By inference, the confinement-induced boundary layer structures are, therefore, responsible only for focusing of the orientational distribution. Indeed, one can confirm this result by observing the tensors $\mathbf{Q}_2$ and $\mathbf{Q}_3$, Eqs. (28) and (29), have major director parallel to the anchoring direction.

To extract a length scale from Eq. (33), one easily calculates the number of nematic layers across the gap, i.e., the number of rotations of the director by π, $[\Delta\psi/\pi]$, which is proportional to $\mathrm{Er}\cdot\mathrm{De}\cdot\mathrm{M}$, where $[\cdot]$ denotes the greatest integer function. It follows that the *average nematic layer length scale is proportional to* $(\mathrm{De}\,M\,E\mathrm{r})^{-1}$, which is the *square of the Marrucci scaling.*

The value of the prefactor $M(a,N,\psi_0)$ affects the number of layers *and the chirality* of director windup. If $M > 0$, the major director rotates clockwise from the top plate to the midgap $y = 0$, then "unwinds" counterclockwise from $y = 0$ to the bottom plate. If $M < 0$, the directors reverse chirality. By changing the molecules from rods ($a > 0$) to platelets ($a < 0$), and by varying ψ_0, it is possible to achieve M of either sign, thereby reversing the direction of rotation.

For *flow-aligning nematic polymers in weak shear*, $|\lambda_L| > 1$, two effects are deduced. First, M may be positive or negative, and indeed $M \equiv 0$ if ψ_0 matches the Leslie alignment angle, $1/2\cos^{-1}(1/\lambda_L)$. This result is quite natural: the long-range permeation structure may be completely suppressed if one preconditions the plates to match the shear-alignment angle of the nematic polymer.

For *tumbling nematic polymers*, $|\lambda_L| < 1$, one finds $M > 0$ and bounded away from zero, implying enhanced layering and smaller lengthscales of director rotation. This result is also natural: a tumbling nematic polymer cannot resist generation of spatial

director distortions no matter what the plate anchoring condition is, since the material has no preferred angle to resonate with.

C. Order parameter structure

We now extract degree and scales of molecular elasticity induced by slow Couette cells. The striking feature is extreme sensitivity to anchoring angle. From the s, β formulas, Eq. (24), and the $\mathbf{Q}$ tensor formulas (26)–(32), it follows that $s^{(1)}$ and $\beta^{(1)}$ *vanish* if and only if $\psi_0 = 0$, $\pi/2$ (mod π). We then carry the expansion to next order (omitted) and find:

1. Tangential anchoring ($\psi_0 = 0$)

Order parameter distortions enter at $O(\mathrm{De}^2)$ through two boundary layers and the long-range permeation structure:

$$s = s_0 + \mathrm{De}^2 s^{(2)} + O(\mathrm{De}^3),$$

$$\beta = \mathrm{De}^2 \beta^{(2)} + O(\mathrm{De}^3),$$

$$s^{(2)} = \left[B_1 \mathrm{Er}(y^2-1) + B_2 \left(\frac{\cosh(\mathrm{Er}^{1/2} D y)}{\cosh(\mathrm{Er}^{1/2} D)} - 1 \right) - B_3 \left(\frac{\cosh(\mathrm{Er}^{1/2} B y)}{\cosh(\mathrm{Er}^{1/2} B)} - 1 \right) \right],$$

$$\beta^{(2)} = \left[B_4 \mathrm{Er}(y^2-1) - 2B_3 \left(\frac{\cosh(\mathrm{Er}^{1/2} B y)}{\cosh(\mathrm{Er}^{1/2} B)} - 1 \right) \right], \tag{34}$$

where

$$B_1 = -\frac{9(\lambda_L - 1)(3\lambda_L - 2)(1 - s_0)(5 + 7s_0)}{N(2+s_0)^2(4s_0 - 1)},$$

$$B_2 = \frac{243}{N^2(2+s_0)^2(4s_0-1)} \left(\mathrm{Er}(\lambda_L - 1)^2 + \frac{(3\lambda_L - 2)(\lambda_L - 1)}{N^2 s_0 (4s_0 - 1)} \right),$$

$$B_3 = \frac{9(1-s_0)}{N(2+s_0)^2} \left(\mathrm{Er}(\lambda_L - 1)^2 + \frac{(3\lambda_L - 2)(\lambda_L - 1)(1 - s_0)}{9 N s_0} \right),$$

$$B_4 = \frac{9(\lambda_L - 1)(3\lambda_L - 2)(1 - s_0)}{N(2+s_0)^2}. \tag{35}$$

Combined with the director results, Eq. (33), we conclude that *tangential anchoring leads to a director-dominated, non-uniform, long-range structure with* Er^{-1} *mean scaling, together with weak, order-parameter modulations on both* $\mathrm{Er}^{-1/2}$ *and* Er^{-1} *scales.*

2. Normal (homeotropic) anchoring ($\psi_0 = \pi/2$)

The structure model (16)–(21) for in-plane $\mathbf{Q}$ tensors admits a symmetry: $(a, \psi) \rightarrow (-a, \pi/2 + \psi)$. This property implies the asymptotic solution with $\psi_0 = \pi/2$ can be obtained directly from Eqs. (34) and (35). *Thus normal and tangential anchoring are quantitatively different, with changes in numerical prefactors, yet qualitatively similar scaling laws*. The figures will illustrate these features.

3. Tilted anchoring ($0 < \psi_0 < \pi/2$ *or* $\pi/2 < \psi_0 < \pi$)

The results above for $\psi_0 = 0,\ \pi/2$ are quite special, as evident from the boundary layer tensors $\mathbf{Q}_2$ and $\mathbf{Q}_3$, formulas (28) and (29). *Any pretilt induces an order parameter response of the same amplitude,* $O(\mathrm{De})$, *as the director distortion,* yet localized in the two boundary layers:

$$s = s_0 + \mathrm{De}\, s^{(1)} + O(\mathrm{De}^2),$$

$$\beta = \mathrm{De}\,\beta^{(1)} + O(\mathrm{De}^2), \tag{36}$$

where [with B and D given above in Eqs. (31) and (32)]

$$s^{(1)} = a \sin 2\psi_0 \left[A_1 \left(\frac{\cosh(\mathrm{Er}^{1/2} B y)}{\cosh(\mathrm{Er}^{1/2} B)} - 1 \right) - A_2 \left(\frac{\cosh(\mathrm{Er}^{1/2} D y)}{\cosh(\mathrm{Er}^{1/2} D)} - 1 \right) \right],$$

$$\beta^{(1)} = 2a \sin 2\psi_0 \left[A_1 \left(\frac{\cosh(\mathrm{Er}^{1/2} B y)}{\cosh(\mathrm{Er}^{1/2} B)} - 1 \right) \right],$$

$$A_1 = \frac{1 - s_0}{6 N s_0} > 0, \quad A_2 = \frac{9}{2 N^2 s_0 (4 s_0 - 1)} > 0. \tag{37}$$

This result is suggestive of a fundamental flow-nematic structure mechanism. When a solid boundary or even a defect structure pins the major director at an angle tilted with respect to the flow–flow gradient axes, molecular elasticity is amplified in a local boundary layers.

D. Penetration depth due to plate anchoring

All asymptotic results, once translated into dimensional gap height y, imply all tensor distortions, Eqs. (26)–(35), have local boundary layer and long-range structure scales that are *independent of the gap separation scale* $2h$. Therefore, there appears to be no ''memory'' of the gap width in the slow-plate scaling properties. This prediction confirms the linearized predictions of Carlsson (1986), and available experimental evidence as discussed by Larson (1999).

III. NUMERICAL RESULTS

Figure 1 depicts the plane shear flow geometry. For the reported computations, we fix a concentration in the nematic regime $N = 6$ and fix the aspect ratio $r = 3$ (i.e., $a = 0.8$), consistent with our complementary studies of the monodomain dynamics problem [Forest and Wang (2003); Forest *et al.* (2003)]. Figures 2–5 compare the exact formulas for the director angle ψ, order parameters s and β, and flow velocity v_x, with direct numerical solutions of the steady, two-point boundary-value problem. Figure 5 also gives shear stress and light scattering intensity predictions. [Selected results are further compared with numerical integration of the full space-time model (7)–(14), restricted to in-plane $\mathbf{Q}$ tensors. All reported steady numerical solutions are stable under these restrictions.]

We begin with confirmation of the formulas for $0 < \mathrm{De} \ll 1$ and $0 < \mathrm{De}\cdot\mathrm{Er} \ll 1$, Fig. 2, where the asymptotic formulas are nearly identical to the numerical solutions. For tangential and normal anchoring, we set $\mathbf{De} = \mathbf{0.1}$, $\mathbf{Er} = \mathbf{1}$; for tilted anchoring, $\psi_0 = \pi/6$, we have to lower $\mathrm{De} = 0.01$ with the same $\mathrm{Er} = 1$ to maintain agreement between the asymptotic formulas and the numerical solutions. These structures

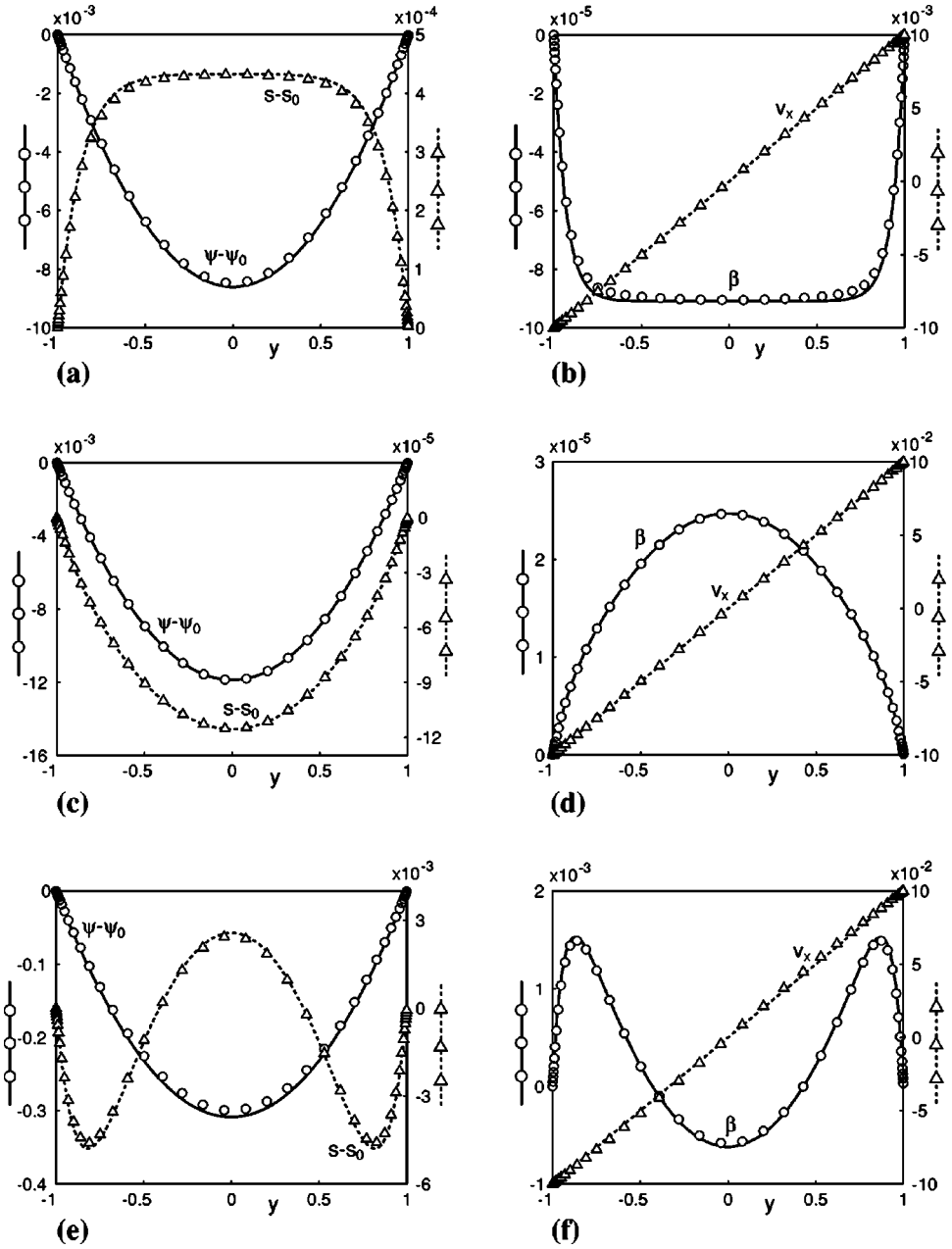

FIG. 2. Comparison of the numerical solutions (circles/triangles) of the steady boundary-value problem and the exact asymptotic formulas (solid/dashed lines). Top row: tilted anchoring ($\psi_0 = \pi/6$) with De = 0.01 and Er = 1. Middle row: parallel anchoring ($\psi_0 = 0$) with De = 0.1 and Er = 1. Bottom row: normal anchoring ($\psi_0 = \pi/2$) with De = 0.1 and Er = 1. In all figures, circles and solid lines use the left (vertcal) axis; triangles and dashed lines use the right axis.

further illustrate subtle effects of ψ_0-dependent numerical prefactors on the order parameters: the boundary layer modes may *align with* [$\psi_0 = 0, \pi/6$; Figs. 2(a)–2(d)] or *oppose* [$\psi_0 = \pi/2$; Figs. 2(e) and 2(f)] the permeation structure. In the latter scenario, a secondary length scale emerges due to the superposition.

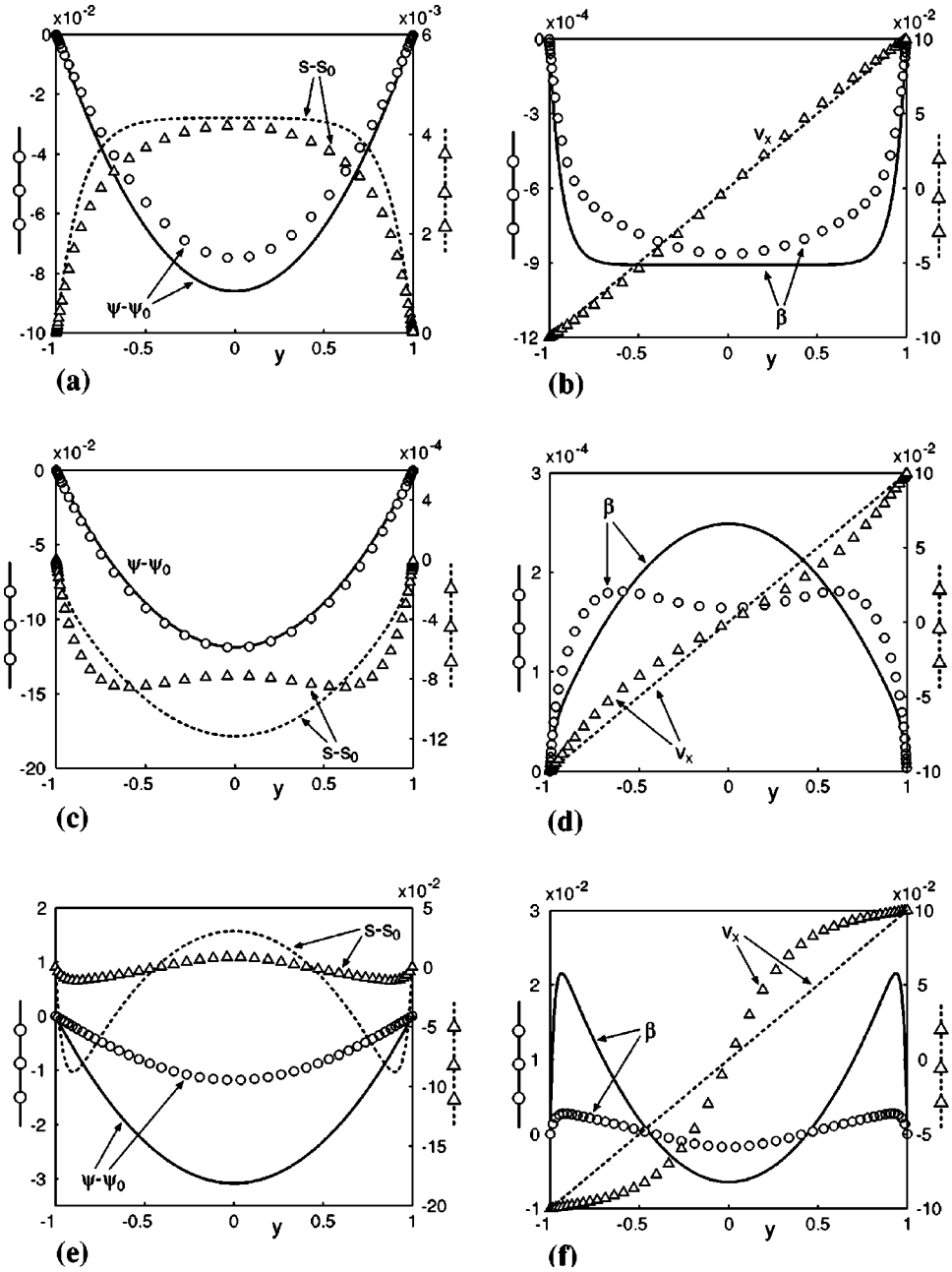

FIG. 3. Comparison of the numerical solutions (circles/triangles) of the steady boundary-value problem and the exact asymptotic formulas (solid/dashed lines). Top row: tilted anchoring ($\psi_0 = \pi/6$) with De = 0.1 and Er = 1. Middle row: parallel anchoring ($\psi_0 = 0$) with De = 0.1 and Er = 10. Bottom row: normal anchoring ($\psi_0 = \pi/2$) with De = 0.1 and Er = 10.

Next, we illustrate breakdown of the asymptotic formulas with direct numerical solutions when *either* of the two asymptotic conditions, $\mathrm{De} \ll 1$ and $\mathrm{Er}\cdot\mathrm{De} \ll 1$, are gradually pushed out of the asymptotic regime. Our purpose here is to *monitor emergence of new, non-asymptotic structures, and to identify sources of additional scaling behavior*.

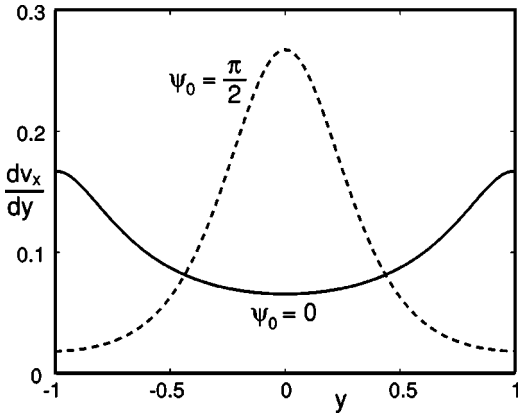

FIG. 4. Comparison of dv_x/dy, which defines a local Deborah number across the plate gap, for parallel anchoring ($\psi_0 = 0$) and normal anchoring ($\psi_0 = \pi/2$) for De = 0.1 and Er = 10. These data are postprocessed from the numerical solutions of the steady boundary-value problem. Note the mean Deborah number across the gap is precisely De, so these structures convey the nematic polymer feedback to the flow.

Figure 3 imposes tangential [(c) and (d)] and normal anchoring [(e) and (f)] with **De = 0.1**, **Er = 10**. The asymptotic formulas still agree to within errors of $O(\mathrm{De}^2)$, yet one finds the emergence of nonlinear velocity structure not captured by the asymptotic formulas. Qualitatively distinct velocity structures are generated for tangential versus normal anchoring. Tangential anchoring yields a local Deborah number, $\partial v_x/\partial y$, that is greater in the plate boundary layers, and lower near the midplane, than the plate-imposed, gap average De = 0.1. This suggests a resonant velocity structure with power law $y^p, p > 1$, p odd. Normal [Fig. 3(f)] and tilted [Fig. 3(b)] anchoring generate the opposite concavity in the flow velocity with apparent power law of the form $y^{1/p}$, $p > 1$, p odd. Figure 4 highlights the stark contrast in local De between tangential and normal anchoring for an otherwise identical experiment, extracted from the numerical velocity data of Figs. 3(d) and 3(f).

For tilted anchoring, Figs. 3(a) and 3(b), a more stringent $\mathrm{Er}\cdot\mathrm{De}$ condition is needed for asymptotic agreement, with **De = 0.1**, **Er = 1**. One finds quantitative asymptotic accuracy, but qualitatively the asymptotic formulas fail to resolve shorter lengthscale structure in the order parameters and velocity, while overestimating the amplitudes of all orientation variables.

In Figs. 5(a) and 5(b), we raise the plate speeds (**De = 0.5**) by a factor of 5 from Fig. 3, with **Er = 10** (for which $\mathrm{De}\cdot\mathrm{Er} = 5$), and present results only with parallel anchoring. *Correlated boundary layers are spawned among v_x and both order parameters*, totally missed by the asymptotic formulas. The numerical solutions convey an *interior*, director-dominated orientation structure, with almost stagnant flow (local $\mathrm{De} \ll 1$) and nearly constant order parameters. *Near the plates*, the flow velocity rapidly transitions to the plate speed, with corresponding high local De, and strong molecular elasticity reflected in the order parameter structure.

We close with predictions of *shear-gap stresses* [Fig. 5(c)] and *light intensity patterns* [Fig. 5(d)] associated with these steady structures. The first normal stress difference appears to correlate with the maximum birefringence parameter, s, with a positive, maximum N_1 at the plates, then a sharp boundary layer transition leads to a *sign change* of N_1 in the boundary layers, then a nearly constant $N_1 \approx 0$, yet negative, across the gap interior. On the other hand, N_2 appears to correlate with the second birefringence param-

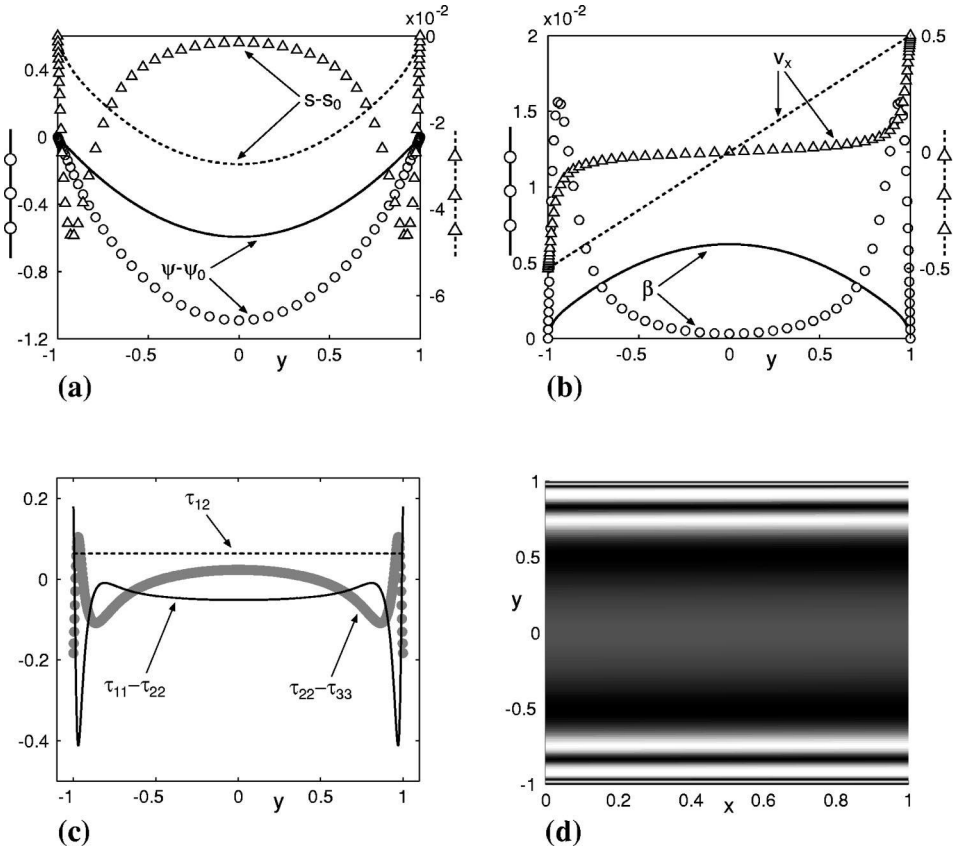

FIG. 5. Top row: Comparison of the numerical solutions (circles/triangles) of the steady boundary-value problem and the exact asymptotic formulas (solid/dashed lines) for parallel anchoring ($\psi_0 = 0$) with De $= 0.5$ and Er $= 10$. Bottom row: Rheological structure profiles associated with the numerical results of the top row. Here, we provide the first ($N_1 = \tau_{11} - \tau_{22}$) and second ($N_2 = \tau_{22} - \tau_{33}$) normal stress differences, the shear stress (τ_{12}), and the light scattering intensity function [Mather *et al.* (1997)], $I = I_0 \sin^2(2\pi a_1 s)$, across the plate gap, where a_1 is the ratio of the sample thickness to the wavelength of incident light. The normalized birefringence s measures the difference between orientation along the flow direction and along the vorticity axis.

eter, β, also with sharp boundary layers near the plates with *2 sign changes* of N_2 in Fig. 5(d). Even in the asymptotic regime (figure not shown), both N_1 and N_2 change sign across the plate gap, so that boundary measurements of N_1, N_2 in steady state are not indicative of internal stress profiles. The relationship between these locked-in stress profiles and mechanical properties of nematic polymer films poses an intriguing challenge.

The light scattering intensity across the plate gap associated with the numerical solutions is given in Fig. 5(d). This intensity pattern can be viewed as a combination of pure nematic patterns of the Doi–Marrucci–Greco theory, Forest *et al.* (2000, 2001), where the flow coupling has led to selection of order-parameter structures near the plates and director structures in the interior.

IV. CONCLUSION

The goals met in this paper are twofold: (i) to extend analytical descriptions of structure scaling laws to include molecular elasticity (order parameter variations) and flow of

nematic polymers, in a self-consistent steady balance with nematic (director) elasticity; and (ii) to document nonasymptotic, yet parametrically controllable, additional structures that emerge as one pulls out of the asymptotic regime. These results serve as a guide for extended numerical studies. Analytically at low De and $De \cdot Er$, the mesoscopic DMG theory predicts that the Marrucci $Er^{-1/2}$ scaling is associated with boundary layer modes residing only in the order parameters, whereas an Er^{-1} mean scaling law appears in non-uniform permeation structures (spanning the entire plate gap). The self-consistent, leading order, flow velocity is a pure linear shear profile. Three incommensurate orientation tensor structures are derived, which together form a source of multiple scales and texture even in the slow flow, small Ericksen number limit.

We confirm the asymptotic formulas with direct numerical simulation of the steady, flow-nematic boundary-value problem of the Doi–Marrucci–Greco model. Pursuant to the question of structures that arise in general flows, we then monitor the breakdown of the asymptotic predictions due to increased plate speed. An intriguing correlation emerges between the molecular plate anchoring conditions and the macroscopic feature of concavity of the flow profile across the entire plate gap. Tangential anchoring leads to a sharp flow gradient near the plates and an interior layer of relatively stagnant flow, whereas any director tilt away from the flow direction reverses concavity of the steady-state flow profile, with a nearly plug-flow layer at each plate and an internal layer with a stronger flow-gradient. These features are controllable either by raising the plate speeds (De) or by promoting distortional versus short-range elasticity (Er), although a systematic study of nonasymptotic scaling behavior remains.

ACKNOWLEDGMENTS

The authors acknowledge private discussion with R. Larson, October, 2002, at the Marrucci Symposium of the Society of Rheology Annual Meeting on the issue of the absense of plate gap height in these scaling properties. Effort sponsored by the Air Force Office of Scientific Research, Air Force Materials Command, USAF, Grant Nos. F49620-02-1-0086 and F49620-03-1-0098; by the National Science Foundation, Grant Nos. DMI-0115445, DMS-0204243, and DMS-0308019; and by the NASA University Research, Engineering and Technology Institute on Bio Inspired Materials (BIMat), Award No. NCC-1-02037.

References

Beris, A. N., and B. J. Edwards, *Thermodynamics of Flowing Systems with Internal Microstructure* (Oxford Science, New York, 1994).

Burghardt, W. R., ''Molecular orientation and rheology in sheared lyotropic liquid crystalline polymers,'' Macromol. Chem. Phys. **199**, 471–488 (1998).

Carlsson, T., ''Theoretical investigation of the shear flow of nematic liquid crystals with the Leslie viscosity $\alpha > 0$: hydrodynamic analogue of first order phase transitions,'' Mol. Cryst. Liq. Cryst. **104**, 307–334 (1984).

Carlsson, T., ''Unit-sphere description of nematic flows,'' Phys. Rev. A **34**, 3393–3404 (1986).

Cladis, P. E., and S. Torza, in *Colloid and Interface Science*, edited by M. Kelker (Academic, New York, 1976), Vol. 4.

de Gennes, P. G., *The Physics of Liquid Crystals* (Clarendon, Oxford, U.K., 1974).

de Gennes, P. G., and J. Prost, *The Physics of Liquid Crystals* (Oxford University Press, Oxford, U.K., 1993).

Doi, M., and S. F. Edwards, *The Theory of Polymer Dynamics* (Oxford University Press, London, 1986).

Donald, A. M., and A. H. Windle, *Liquid Crystalline Polymers*, Cambridge Solid State Science Series (Cambridge University Press, Cambridge, U.K., 1992).

Feng, J., G. Sgalari, and L. G. Leal, ''A theory for flowing nematic polymers with orientational distortion,'' J. Rheol. **44**, 1085–1101 (2000).

Forest, M. G., and Q. Wang, ''Monodomain response of finite-aspect-ratio macromolecules in shear and related linear flows,'' Rheol. Acta **42**, 20–46 (2003).

Forest, M. G., Q. Wang, and H. Zhou, ''Exact banded patterns from a Doi–Marrucci–Greco model of nematic liquid crystal polymers,'' Phys. Rev. E **61**, 6655–6662 (2000).

Forest, M. G., Q. Wang, and H. Zhou, ''Methods for the exact construction of mesoscale spatial structures in liquid crystal polymers,'' Physica D **152-153**, 288–309 (2001).

Forest, M. G., R. Zhou, and Q. Wang, ''Full-tensor alignment criteria for sheared nematic polymers,'' J. Rheol. **47**, 105–127 (2003).

Hinch, E. J., and L. G. Leal, ''The effect of Brownian motion on the rheological properties of a suspension of nonspherical particles,'' J. Fluid Mech. **52**, 683–712 (1972).

Kuzuu, N., and M. J. Doi, ''Constitutive equation for nematic liquid crystals under weak velocity gradient derived from a molecular kinetic equation,'' J. Phys. Soc. Jpn. **52**, 3486–3494 (1983).

Kuzuu, N., and M. J. Doi, ''Constitutive equation for nematic liquid crystals under weak velocity gradient derived from a molecular kinetic equation. II. Leslie coefficients for rodlike polymers,'' J. Phys. Soc. Jpn. **53**, 1031–1040 (1984).

Kupferman, R., M. Kawaguchi, and M. M. Denn, ''Emergence of structure in a model of liquid crystalline polymers with elastic coupling,'' J. Non-Newtonian Fluid Mech. **91**, 255–271 (2000).

Larson, R. G., ''Roll-cell instabilities in shearing flows of nematic polynomials,'' J. Rheol. **37**, 175–197 (1993).

Larson, R. G., *The Structure and Rheology of Complex Fluids* (Oxford University Press, Oxford, U.K., 1999).

Larson, R. G., and D. W. Mead, ''Development of orientation and texture during shearing of liquid-crystalline polymers,'' Liq. Cryst. **12**, 751–768 (1992).

Larson, R. G., and D. W. Mead, ''The Ericksen number and Deborah number cascade in sheared polymeric nematics,'' Liq. Cryst. **15**, 151–169 (1993).

Maffettone, P. L., A. M. Sonnet, and E. G. Virga, ''Shear-induced biaxiality in nematic polymers,'' J. Non-Newtonian Fluid Mech. **90**, 283–297 (2000).

Manneville, P., ''The transition to turbulence in nematic liquid crystals. Part 1. General review. Part 2. On the transition via tumbling,'' Mol. Cryst. Liq. Cryst. **70**, 223–250 (1981).

Marrucci, G., ''Tumbling regime of liquid-crystalline polymers,'' Macromolecules **24**, 4176–4182 (1991).

Marrucci, G., and F. Greco, ''The elastic constants of Maier-Saupe rodlike molecular nematics,'' Mol. Cryst. Liq. Cryst. **206**, 17–30 (1991).

Marrucci, G., and F. Greco, ''Flow behavior of liquid crystalline polymers,'' Adv. Chem. Phys. **86**, 331–404 (1993).

Mather, P. T., A. Romo-Uribe, C. D. Han, and S. S. Kim, ''Rheo-optical evidence of a flow-induced isotropic-nematic transition in a thermotropic liquid-crystalline polymer,'' Macromolecules **30**, 7977–7989 (1997).

Rey, A. D., and M. M. Denn, ''Dynamical phenomena in liquid-crystalline materials,'' Annu. Rev. Fluid Mech. **34**, 233–266 (2002).

Sgalari, G., G. L. Leal, and J. Feng, ''The shear flow behavior of LCPs based on a generalized Doi model with distortional elasticity,'' J. Non-Newtonian Fluid Mech. **102**, 361–382 (2002).

Tan, Z., and G. C. Berry, ''Studies on the texture of nematic solutions of rodlike polymers. 3. Rheo-optical and rheological behavior in shear,'' J. Rheol. **47**, 73–104 (2003).

Tsuji, T., and A. D. Rey, ''Effect of long range order on sheared liquid crystalline polymers. Part 1: Compatibility between tumbling behavior and fixed anchoring,'' J. Non-Newtonian Fluid Mech. **73**, 127–152 (1997).